Research Square

Preprints are preliminary reports that have not undergone peer review.
They should not be considered conclusive, used to inform clinical practice,
or referenced by the media as validated information.

Zero-dimensional perovskite layer-based PSCs for high Voc ~ 1.4 volt: Combination of DFT and OghmaNano Software

Darko A. Noori

darko.noori@univsul.edu.iq

University of Sulaymaniyah

Research Article

Keywords: 3D-CsGeCl3, double-Cs2InCoCl6, 0D-Cs3BiBr6, OghmaNano Simulator, Perovskite Solar Cells, Voltage Losses

Posted Date: November 12th, 2026

DOI: https://doi.org/10.21203/rs.3.rs-8689117/v1

License: This work is licensed under a Creative Commons Attribution 4.0 International License.
Read Full License

Additional Declarations: No competing interests reported.

Zero-dimensional perovskite layer-based PSCs for high Voc ~ 1.4 volt: Combination of DFT and OghmaNano Software

Darko A. Noori

Department of Physics, College of Science, University of Sulaimani, Sulaymaniyah, 46001, Kurdistan Region, Iraq

Corresponding Author: Darko A. Noori

e-mail: darko.noori@univsul.edu.iq

Abstract

In this study, numerical simulations conducted using the OghmaNano software are employed to investigate the impact of incorporating the zero-dimensional (0D) Cs_3BiBr_6 perovskite material into a multi-layered, three-dimensional (3D) structure composed of $CsGeCl_3$ and double $Cs_2InCoCl_6$ perovskite materials. The various dimensions of perovskite materials, including three-dimensional, double perovskite, and zero-dimensional structures, are used in the construction of perovskite solar cells (PSCs). The triple-layer architecture's analysis, including charge transport, carrier generation (G), recombination (R), light absorption, and reflection, were all simulated using the finite-difference drift-diffusion method. A detailed optical study shows that inserting a 50-nm thick 0D-Cs_3BiBr_6 layer improves the process of converting light into electricity. It helps the material absorb more light in the visible region and minimizes the amount of light that bounces off. Furthermore, results show that the 0D perovskite improves the extraction of charge carriers, reduces recombination at the interface, and increases the built-in electric potential due to a higher concentration of charge carriers (n). These factors collectively lead to a significant increase in the open-circuit voltage (V_{oc}). When compared to the bi-layer cell design (3D-$CsGeCl_3$/double-$Cs_2InCoCl_6$), the resulting tri-layer device structure shows better photovoltaic performance. The findings indicate that integrating low-dimensional perovskites can enhance the open-circuit voltage, increasing it to 1.36 V. Additionally, Cs_3BiBr_6 is identified as a potential material for creating next-generation perovskite solar cells that are both highly efficient and stable. The optimized device architecture, which consists of 50 nm $CsGeCl_3$, 200 nm Cs2InCoCl6, and 50 nm Cs_3BiBr_6, achieves a champion power conversion efficiency (PCE) of 33.15%.

Keywords: 3D-$CsGeCl_3$, double-$Cs_2InCoCl_6$, 0D-Cs_3BiBr6, OghmaNano Simulator, Perovskite Solar Cells, Voltage Losses

1. Introduction:

The main structure of perovskite solar cells includes an absorber layer that is placed between layers responsible for transporting electrons and holes. Within these parts, the absorb layer is especially important because it absorbs incoming light and creates electron-hole pairs (Sahoo et al. 2018). The physical, electronic, and optical characteristics of this layer are crucial in affecting how well the entire device performs.

Because of their exceptional optoelectronic properties, inorganic perovskite materials like $CsPbX_3$ (X = Cl, Br, I) have gained significant interest among researchers for use in energy harvesting applications (Chen et al. 2018). However, a few obstacles prevent their widespread use, notable among them being the toxicity of lead, which restricts large-scale uses. Lead-free substitutes for $CsPbX_3$ in solar cells and associated technologies, such as $CsGeX_3$ (X = Cl, Br, I), have emerged as promising solutions to address this challenge. Many interesting characteristics and new aspects of these compounds have been thoroughly investigated using both theoretical and experimental methods. For example, $CsGeCl_3$ and $CsGeBr_3$ exhibit a notable red shift during compression and extremely sensitive absorption edges to external hydrostatic pressure (Qu et al. 2025). Depending on the computational technique used, the reported band gap values of $CsGeX_3$ materials, which are classified as direct band gap semiconductors, range from 0.82 to 7.91 eV (Sharma et al. 2024)(Seo et al. 1998)(Azeem et al. 2025). The $CsGeI_3$, $CsGeBr_3$, and $CsGeCl_3$ have band gaps of 1.19, 1.46, and 2.13 eV, respectively, according to standard estimates. Using the hybrid functional (HSE) model increases the accuracy of these predictions, yielding band gap values of 1.64, 2.34, and 3.24 eV for $CsGeI_3$, $CsGeBr_3$, and $CsGeCl_3$, respectively (Thi Han et al. 2022a). To improve the performance of PSCs, several methodologies have been set up, such as functional layer modification, tandem structure design, and interface and defect passivation. However, the pursuit of novel perovskite materials continues to be a more straightforward and successful strategy.

Due to their exceptional stability and adjustable optoelectronic characteristics, environmentally friendly, lead-free double halide perovskites with the general formula A_2BX_6 have garnered a lot of attention lately (Faizan et al. 2024)(Faizan et al. 2021)(Barichello et al. 2024). Monovalent (B^+) and trivalent (B^{3+}) ions can be used in place of the B-site tetravalent cation in these materials, allowing for a wide range of combinations and providing chances to manipulate their physical characteristics through synthetic design. For example, Cs_2AgBiX_6 (where X is either Cl or Br) has

been described as a stable double perovskite with extended carrier recombination lifetimes and significant light absorption; yet its photovoltaic efficiency may be limited by its indirect band structure and relatively wide band gap (chrafih et al. 2023)(Tripathi et al. 2019). The family of double perovskites has been expanded by proposing additional trivalent ions, including Sb^{3+}, In^{3+}, and Tl^{3+} as replacements for Bi^{3+}. Interestingly, two direct-gap compounds with band gaps close to 1.0 eV, $Cs_2InSbCl_6$ and $Cs_2InBiCl_6$ (Zhou et al. 2018)(Alnujaim et al. 2022), have shown efficiencies have demonstrated efficiencies comparable to those of $MAPbI_3$.

Furthermore, Double perovskite materials, such as Cs_2InSbI_6, Cs_2InGaX_6, and Cs_2InCoX_6, have been widely explored for their promising optoelectronic properties. It has been determined that Cs_2InSbI_6 is a promising option with a high potential for use in commercial energy applications. The optoelectronic characteristics of Cs_2InGaX_6 (X = Cl, Br, I) have been extensively investigated in recent research, underscoring the adaptability of this group of double halide perovskites (Kibbou et al. 2021). According to the results of theoretical research, Cs_2InCoX_6 perovskites are excellent prospects for photovoltaic and optoelectronic applications because of their exceptional stability, direct band gaps, and advantageous absorption properties that complement the solar spectrum (Luo et al. 2018).

At present, although there have been many studies on 2D and 3D halogenated perovskite materials, few have investigated the properties of 0D materials. Recently, 0D Cs_3BiX_6 (X = Br, Cl) was experimentally synthesized (Yang et al. 2022). The crystal structure of Cs_3BiX_6 (X = Br, Cl) belongs to a monoclinic system with space group C_2/c and is composed of cations Cs^+, which lose electrons, and the $[BiX_6]_3$- group, which obtains electrons (Liang et al. 2021). In this simulation research paper, we investigated the effect of the zero-dimensional perovskite material (Cs_3BiBr_6) on the open circuit voltage of the cell and overall efficiency of the cell in the structure of 50-nm $CsGeCl_3$/200-nm $Cs_2InCoCl_6$/50-nm Cs_3BiBr_6 based new approach of PSCs structure. This structure stands for 3D/Double/0D perovskite material structure between the two contact layers FTO and Au, without electron and hole transporting layer materials, as shown in Figure 1. At the end, this study also focuses on the light absorption, electron-hole generation, and transportation in and via perovskite materials to achieve a novel structure of perovskite solar cell for high efficiency and stability with low cost.

2. Device Structure and Simulation Method:

For this theoretical study, a multilayer PSCs architecture was designed to exploit the complementary advantages of mixed perovskite dimensionalities within ultrathin layers. As shown in Figure 1, the device employs a 50-nm fluorine-doped tin oxide (FTO) front electrode, providing high optical transparency and sufficient electrical conductivity for efficient electron collection. Beneath the FTO, a 50-nm three-dimensional (3D) $CsGeCl_3$ perovskite layer functions simultaneously as an electron transport layer (ETL) and a UV-active absorber, benefiting from favorable band alignment and high carrier mobility to facilitate rapid electron extraction.

The main absorber consists of a 200-nm double perovskite $Cs_2InCoCl_6$ layer, chosen for its reduced toxicity compared with Pb-based perovskites, enhanced chemical stability, and strong absorption in the UV–visible region. This layer serves as the main photogeneration medium, producing free carriers under illumination. On the hole-transport side, a 50-nm zero-dimensional (0D) Cs_3BiBr_6 perovskite layer acts as the hole transport layer (HTL), offering strong defect tolerance, efficient hole extraction, and effective electron blocking to suppress interfacial recombination. A 100-nm gold electrode completes the device as a stable back contact for hole collection.

The integration of 3D, double, and 0D perovskite layers enables a synergistic balance between light absorption, charge generation, carrier transport, and interfacial stability. The 3D $CsGeCl_3$ ETL promotes efficient electron injection, the double perovskite $Cs_2InCoCl_6$ ensures broad spectral absorption with improved intrinsic stability, and the 0D Cs_3BiBr_6 HTL minimizes trap-assisted recombination while enhancing back-contact passivation. The device was conceptually designed and numerically simulated using OghmaNano to evaluate its optical and electrical performance, highlighting the potential of dimensionality-engineered perovskite heterostructures for next generation photovoltaic applications.

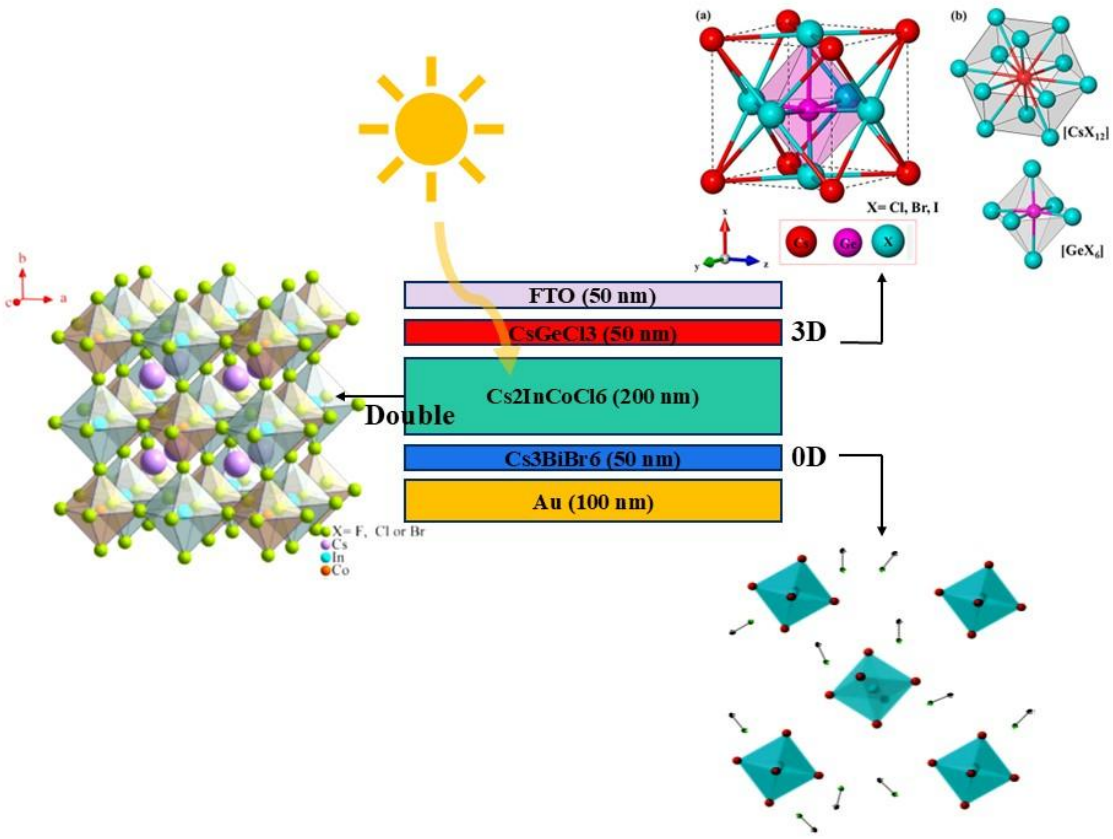


Figure 1. Simulated device structure of the perovskite solar cell using OghmaNano software. The cell is composed of five layers: three perovskite layers and two contact layers. The active layer adopts a double perovskite structure ($Cs_2InCoCl_6$), while the electron transport layer is modeled as a three-dimensional perovskite ($CsGeCl_3$), and the hole transport layer as a zero-dimensional perovskite (Cs_3BiBr_6).

Figure 2(a) shows the simulated AM1.5G solar spectrum used as the illumination source in the OghmaNano model, spanning wavelengths from 300 to 900 nm. The spectrum exhibits a peak intensity of approximately 1.5×10^6 Wm^{-2} within the visible region (400 - 750 nm), where perovskite absorbers possess strong optical absorption, ensuring efficient photon harvesting and electron-hole pair generation across the active layers. The insect of Figure 2(b) presents a schematic of the device architecture, illustrating the transmission of incident sunlight through the transparent FTO electrode and its subsequent absorption within the multilayer perovskite stack.

The interfacial energy-level alignment plays a critical role in governing carrier transport and recombination. As depicted in Figure 2(b), the 3D $CsGeCl_3$ layer absorbs high-energy UV photons while simultaneously functioning as the electron transport layer (ETL), thereby facilitating efficient electron extraction. The double perovskite $Cs_2InCoCl_6$ acts as the primary absorber,

contributing dominant photon absorption and carrier generation throughout the visible spectrum. In contrast, the 0D Cs_3BiBr_6 layer serves as a selective hole transport layer, promoting hole extraction toward the Au back contact while effectively blocking electron leakage.

This cascaded band alignment enhances charge separation and suppresses interfacial recombination. Together, the AM1.5G spectrum in Figure 2(a) and the device schematic in Figure 2(b) underscore the deliberate integration of optical absorption and energy-band engineering, validating the effectiveness of the dimensionality-engineered (3D/double/0D) perovskite heterostructure for efficient light harvesting and charge extraction.

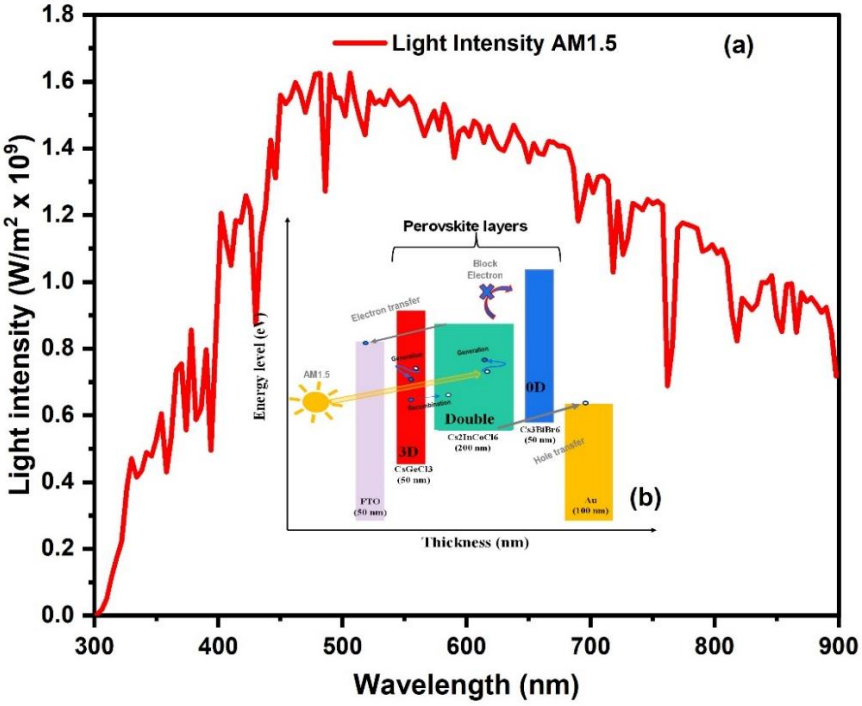


Figure 2. (a) Simulated light intensity spectrum for air mass AM1.5, used as the illumination source in the OghmaNano simulator, and (b) schematic of the perovskite layer structure, showing the energy levels and thicknesses of the layers. Electron-hole pairs are generated within the perovskite layers and subsequently transported to the contacts.

The perovskite materials used in this cell structure were obtained from theoretical research (Cs_3BiBr_6 (Liang et al. 2021), $CsGeCl_3$ (Thi Han et al. 2022b), and $Cs_2InCoCl_6$ (Tang et al. 2022)) and inserted into the OghmaNano simulator. For this purpose, their specific properties, particularly the refractive index, absorption coefficient, and energy gaps, were analyzed, as shown in Figure 3 and Table 1. The absorption coefficient spectra (Figure 3a) reveal that Cs_3BiBr_6 (0D) exhibits

strong absorption (~ $8x10^5$ 1/cm) in the ultraviolet region (0-300 nm) and it transparent to the high wavelength, while $CsGeCl_3$ (3D) dominates (~ $4x10^5$ 1/cm) in the range 300-400 nm, and $Cs_3InCoCl_6$ (double perovskite) contributes ($0.5x10^5$ 1/cm) primarily to the longer wavelength region 400-800 nm, highlighting the complementary optical response of the heterostructure. The refractive index profiles (Figure 3b) further indicate distinct dispersion behaviors for each material, with $Cs_2InCoCl_6$ showing a steady increase (~ 2.5 a.u) at higher wavelengths while the 3D and 0D perovskite goes to steady (~ 1.75 and 1.45 a.u, respectively) from 400 nm to longer wavelength and become transparent in the visible region, consistent with its role in extending light interaction and trapping within the absorber layer. Together, these optical features justify the layered configuration of the device, where each perovskite contributes synergistically to broad-spectrum photon harvesting and efficient charge carrier generation (Najarpour and Matloub 2025).

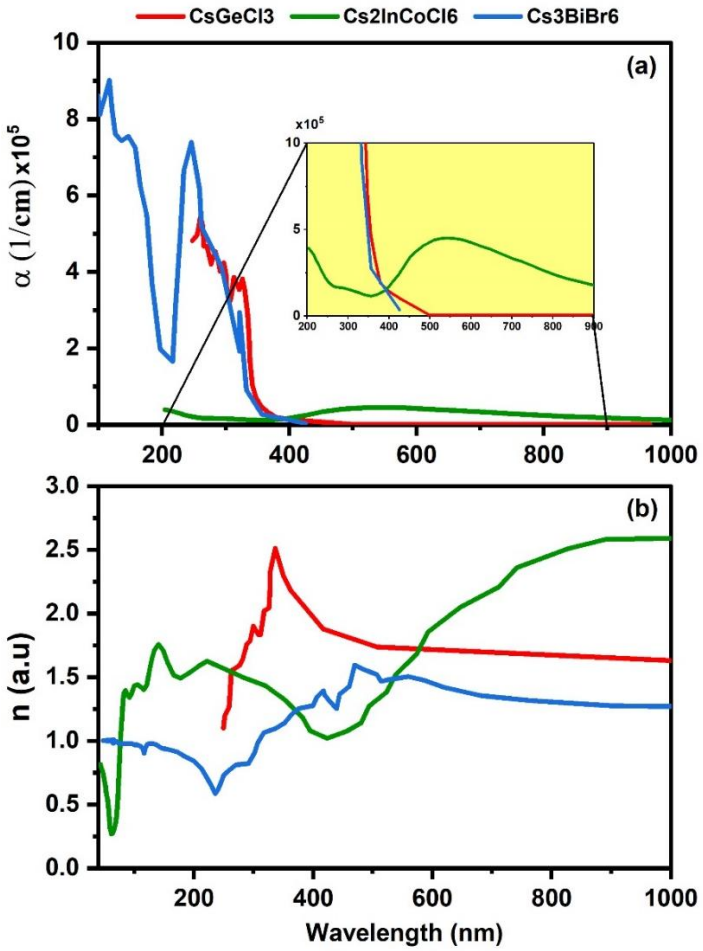


Figure 3. (a) Absorption coefficient spectrum and (b) refractive index of $CsGeCl_3$, $Cs_2InCoCl_6$, and Cs_3BiBr_6, corresponding to 3D, double, and 0D perovskite material structures, respectively. The results are obtained from density functional theory (DFT) simulations for wavelengths in the range of 0-1000 nm.

The OghmaNano software was originally developed as a simulation tool for photovoltaic (PV) devices based on organic and PSCs (Mäckel and MacKenzie 2018). A key advantage of this model is its efficient treatment of Shockley-Read-Hall (SRH) carrier trap states (Shockley and Read 1952) and the management of electrical mesh points. The software relies on standard physical models, including the bipolar drift-diffusion framework, to describe the current flux density of electrons and holes, expressed as:

$$J_n = q\mu_c n \frac{\partial E_c}{\partial x} + qD_n \frac{\partial n}{\partial x} \tag{1}$$

$$J_p = q\mu_n p \frac{\partial E_v}{\partial x} - qD_p \frac{\partial p}{\partial x} \tag{2}$$

Here, J_n and J_p represent the electron and hole flux densities, respectively; q is the elementary charge; n and p are the free electron and hole concentrations; μ_n and μ_p denote the electron and hole mobilities; D_n and D_p are the electron and hole diffusion coefficients; and E_c and E_v correspond to the conduction and valence band mobility edges. Also, the equation of continuity for electrons and holes in position space indicates as follows:

$$\frac{\partial J_n}{\partial x} = q\left(R_n - G + \frac{\partial n}{\partial x}\right) \tag{3}$$

$$\frac{\partial J_p}{\partial x} = -q\left(R_p - G + \frac{\partial p}{\partial x}\right) \tag{4}$$

where R_n and R_p are the net recombination rate, and G is the free carrier generation rate. As well as the Poisson equation for calculating the internal electrostatic potential is given by,

$$\frac{d}{dx}\varepsilon_o \varepsilon_r \frac{\partial \varphi}{\partial x} = q(n - p) \tag{5}$$

where ε_o is the permittivity of the vacuum, ε_r is the relative permittivity, and φ denotes the voltage profiles. Furthermore, a detailed explanation of an equation model for typical solar cells can be found in the references (Hwang et al. 2009)(Piprek 2017)(Richardson and Walker 2016)(Johnston and Herz 2016a)(Johnston and Herz 2016a). The model employs SRH formalism to describe the recombination and trap states for a better understanding of the rates at which electrons and holes can escape or become captured in carrier traps reported in. The equations to estimate the parameters of the solar cell, such as Voc, FF, and PCE, can be written as (Bothe et al. 2023)(Marzouglal et al. 2024)(Gupta et al. 2010),

$$V_{oc} = \frac{nkT}{q} \ln\left[\frac{J_{sc}}{J_o} + 1\right] \quad (6)$$

$$FF = \frac{J_{mp}V_{mp}}{J_{Sc}V_{oc}} \quad (7)$$

$$\eta = \frac{p_m}{p_{in}} = \frac{(J_{sc} \times V_{oc} \times FF)}{P_{in}} \quad (8)$$

where V_{oc} and J_{sc} represent the open-circuit voltage and short-circuit current density, respectively, J_o is a saturation current density, T is an absolute temperature, k is a Boltzmann constant, J_{mp} and V_{mp} are the current and voltage density at the maximum point, P_m is the maximum output power, P_{in} is the input power, and FF is a fill factor. Thus, the PCE of the devices between the mentioned structures was compared. The electrical and optical parameters of the layer used for the simulated solar cells are shown in Table 1.

Table 1. Simulated solar cell parameters that are used in this research simulation method.

Parameters	$CsGeCl_3$	$Cs_2InCoCl_6$	Cs_3BiBr_6
Optimized Thickness (nm)	50	200	50
Electron mobility (m^2/V.s)	0.0002	0.002	0.0002
Hole mobility (m^2/V.s)	0.0002	0.002	0.0002
Effective density of electron states (m^{-3})	$1x10^{25}$	$1x10^{25}$	$1x10^{25}$
Effective density of hole states ($m^{-3)}$	$1x10^{25}$	$1x10^{25}$	$1x10^{25}$
Free electron to free hole recombination rate constant ($m^{-3}.s^{-1}$)	$1x10^{-15}$	$1x10^{-26}$	$1x10^{-15}$
Electron affinity (eV)	4.0	4.3	2.6
Energy gap (eV)	2.12	1.13	2.5
Relative permittivity (a.u.)	3.4	7.0	5

3. Results and Discussions:

Modeling light scattering, reflection, and absorption in complex material structures has become increasingly significant for a wide range of practical applications, such as solar cells, surface plasmon resonance sensors, photodetectors, and optically tunable liquid crystal surfaces (Ai et al. 2022). In this study, we concentrate on analyzing the optical and electrical characteristics of the cell structure. The light waste due to reflection happens in the layers of the cell, while the primary loss of light occurs due to reflection from the cell's front surface. At longer wavelengths ($\lambda > 500$ nm), any unabsorbed light is redirected back by the back contact layer at the bottom.

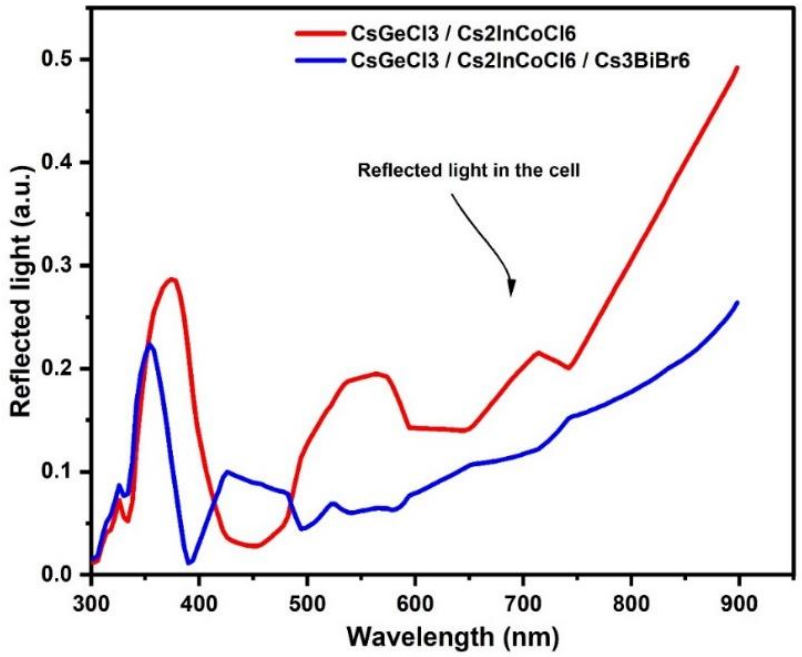


Figure 4. Reflected light in the perovskite solar cell for two different structures: $CsGeCl_3/Cs_2InCoCl_6$ and $CsGeCl_3/Cs_2InCoCl_6/Cs_3BiBr_6$, representing configurations without and with a zero-dimensional perovskite layer, respectively. Overall, the reflection decreases with the incorporation of the 0D perovskite material.

The reflected light spectra of the two structures of the cell: a bilayer structure composed of $CsGeCl_3/Cs_2InCoCl_6$ (red line) and a tri-layer structure that additionally incorporates 0D-Cs_3BiBr_6 (blue line) as shown in Figure 4. The reflection intensity is plotted against wavelength in the range of 300-900 nm in the cell. Overall, the light reflection is low for both structures. In the ultraviolet region 375 nm and across the visible region, the tri-layer cell with the zero-dimensional Cs_3BiBr_6 layer consistently exhibits lower reflectance compared to the bilayer device. This reduction is

particularly notable beyond 500 nm, where the reflected signal in the bilayer continues to rise, peaking above 0.5 a.u. near 900 nm, while the tri-layer remains significantly suppressed. The trend indicates that the addition of Cs_3BiBr_6 enhances light trapping, enhances efficiency of light absorption, and reduces backscattering within the cell (Hao et al. 2018). In the ultraviolet region (300-400 nm), characteristics display sharp fluctuations of strong optical absorption edges. However, the tri-layer device stabilizes lower reflection levels more quickly than the bilayer, suggesting better antireflective behavior. Overall, the results confirm that incorporating the zero-dimensional Cs_3BiBr_6 material effectively suppresses reflectance across a broad spectral range.

This improvement implies more efficient photon harvesting within the active layers, which can contribute to enhancing charge carrier population and preventing recombination within the device. Enhancing charge carrier control, strongly linked to both the fill factor and open-circuit voltage, offers a route to boosting the performance of perovskite solar cells and moving closer to their theoretical efficiency limit (Yang et al. 2015)(Shi et al. 2018a).

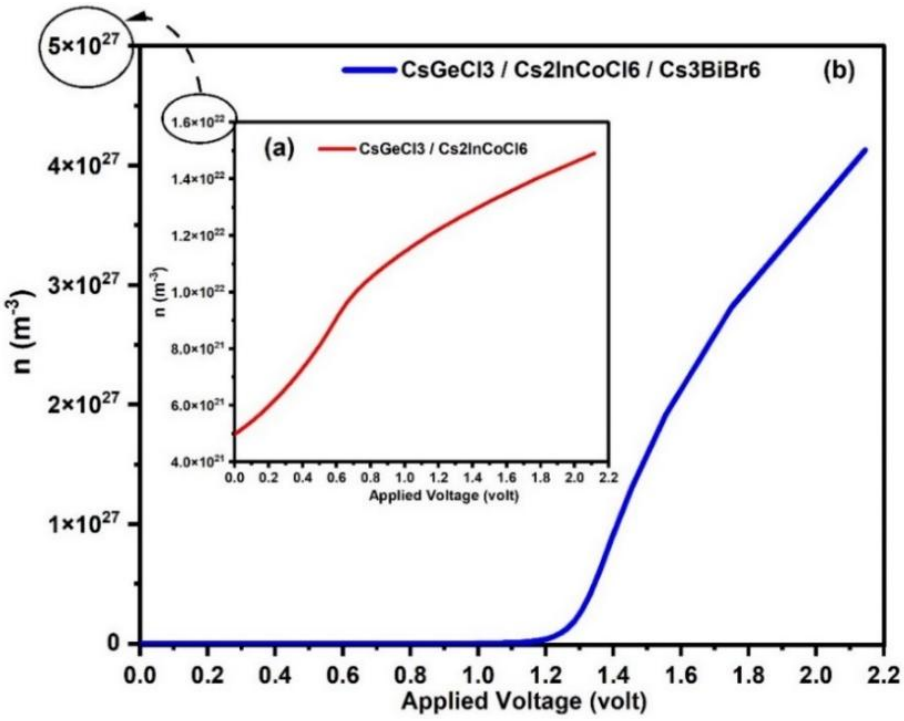


Figure 5. Measured total charge carrier density (n) for the cell structures (a) 3D/Double and (b) 3D/Double/0D. The graphs depict the variation of charge carrier density (y-axis) with respect to the applied voltage (x-axis). The results indicate that the inclusion of the zero-dimensional perovskite layer enhances and stabilizes the charge carrier density.

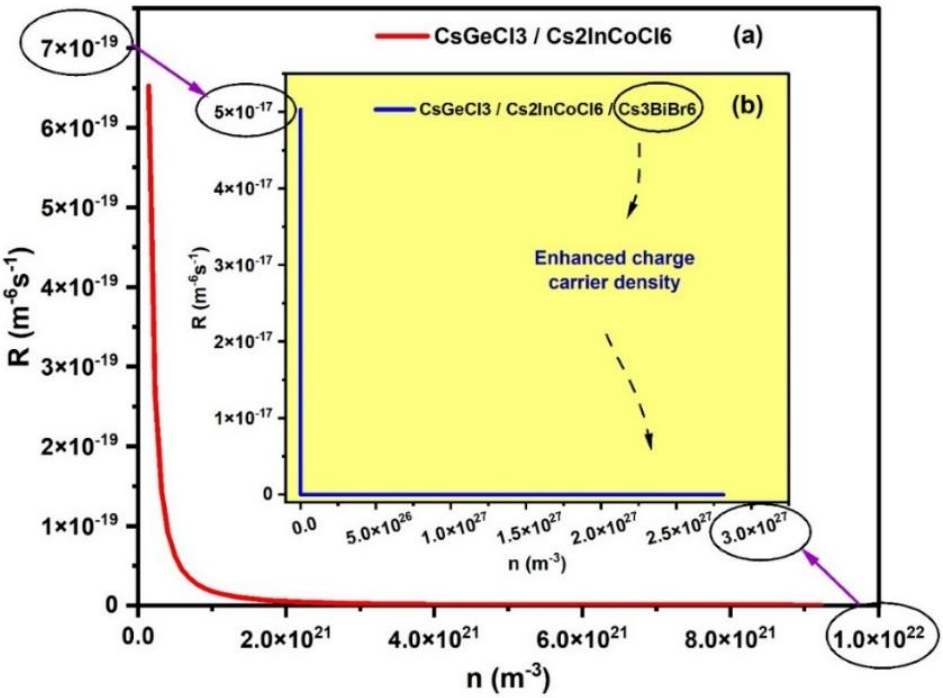


Figure 6. The charge carrier recombination rate in the bulk cell for the two different structures: (a) without and (b) with a zero-dimensional perovskite layer. The comparison illustrates the effect of the 0D perovskite on recombination dynamics within the cell.

In fact, applying a light-trapping structure greatly alters the distribution of carrier generation within the solar cell (Zhu et al. 2023)(Wang et al. 2016). Figure 5 demonstrates the influence of incorporating a 0D perovskite layer on charge carrier accumulation within the device. It is apparent that charge carrier density increases exponentially as a function of voltage according to this relationship $n = n_o e^{\gamma V_{oc}}$ (Maurano et al. 2011). The bilayer structure ($CsGeCl_3/Cs_2InCoCl_6$) exhibits a gradual increase in carrier density with applied voltage, reaching approximately 1.6x10^{22} m^{-3} at 2.2 V. In contrast, the tri-layer structure ($CsGeCl_3/Cs_2InCoCl_6/Cs_3BiBr_6$) shows a sharp and substantial increase beyond 1.2 V, achieving a significantly higher carrier density of up to 5x10^{27} m^{-3}. This enhanced and more stable carrier accumulation can be attributed to the suppression of recombination pathways, as supported by the recombination analysis in Figure 6. The addition of the Cs_3BiBr_6 layer effectively reduces the bulk recombination rate across the entire carrier density range, enabling sustained charge buildup. This improvement reflects the role of the 0D perovskite layer in defect passivation and carrier confinement (Zhao et al. 2023).

The light-harvesting efficiency of these devices remains constrained by significant charge carrier recombination. The variation of charge carrier recombination rate (R) as a function of carrier

density (n) for two device configurations is shown in Figure 6. The difference between the two plots highlights the influence of the additional 0D Cs_3BiBr_6 layer on bulk recombination behavior. In the bilayer structure (Figure 6a), recombination decreased dramatically (from $7x10^{-19}$ m^6 s^{-1} to zero rate) at very low carrier densities ($1x10^{22}$ m^{-3}). However, the recombination rate rapidly decreases as the carrier concentration increases and reaches stable levels soon at higher carrier densities ($2.5x10^{27}$ m^{-3}). This behavior indicates strong recombination losses that limit the accumulation of carriers, thereby constraining device performance. The inset highlights that R in this case remains significantly lower, with maximum values near $5x10^{-17}$ m^6s^{-1}, while also sustaining higher carrier densities, up to ~ $3x10^{27}$ m^{-3}. The total charge carrier recombination rate in perovskite materials depends strongly on the carrier density and can be described as the sum of first-, second-, and third-order processes: $R(n) = k_1n+k_2n^2+k_3n^3$. The first-order term corresponds to trap-assisted (Shockley–Read–Hall) non-radiative recombination and dominates at low carrier densities, reflecting the influence of defect states and material quality. The second-order term represents bimolecular band-to-band radiative recombination, which becomes dominant at intermediate, solar-relevant carrier densities. At very high carrier densities, the third-order term associated with Auger recombination prevails (Johnston and Herz 2016b). This suggests that the inclusion of the 0D Cs_3BiBr_6 layer effectively suppresses recombination pathways, enabling greater carrier accumulation within the device. This result contributes to longer carrier lifetimes, increased diffusion lengths, and ultimately higher photocurrent generation (Kaphle et al. 2020).

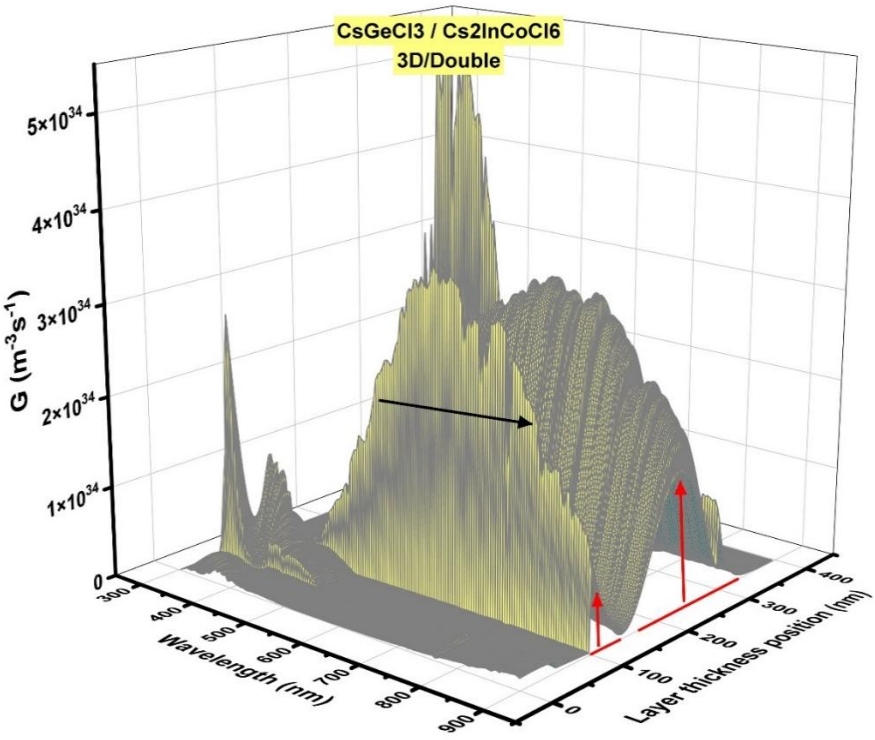


Figure 7. Photon absorption distribution in the perovskite solar cell, showing how charge carrier generation varies with photon wavelength and across the layer thickness positions for the cell structure of 3D/Double.

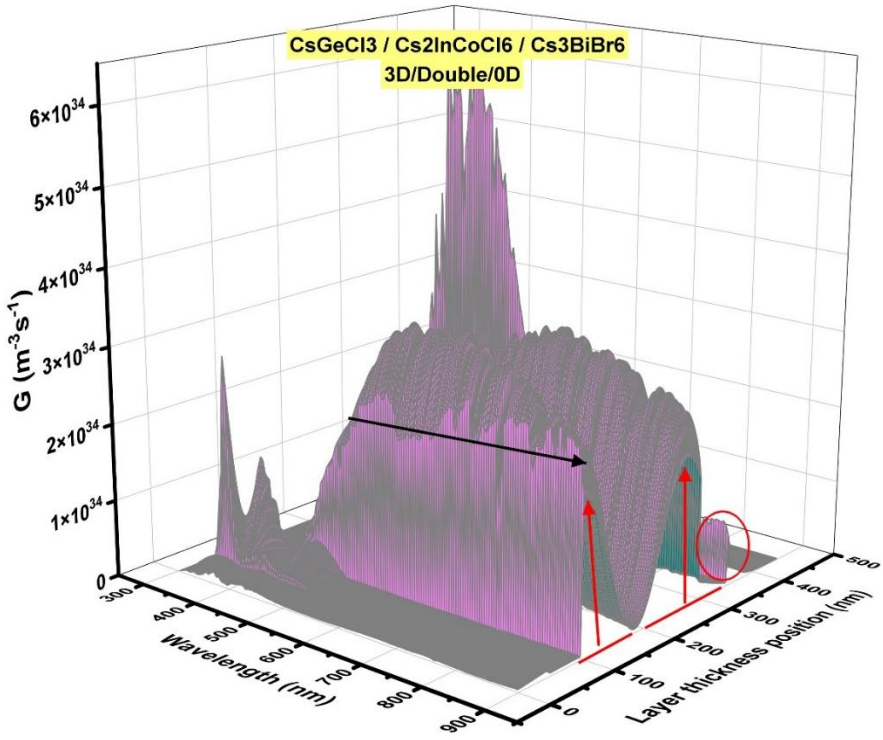


Figure 8. Photon absorption distribution in the perovskite solar cell, showing how charge carrier generation varies with photon wavelength and across the layer thickness positions for the cell structure of 3D/Double/0D

The generation of charge carriers in semiconductors through photon absorption depends primarily on the incident light intensity, surface reflectance, and the absorption coefficient of the material (Shahivandi 2025). From Figures 7 and 8, the optical generation profile of the $CsGeCl_3/Cs_2InCoCl_6$ (3D/Double) and $CsGeCl_3/Cs_2InCoCl_6/Cs_3BiBr_6$ (3D/Double/0D) heterostructures demonstrates strong carrier generation predominantly in the wavelength regions 300-400 nm localized at 100 nm layer thickness (it is related to 3D perovskite material structure), wavelength region 400-900 nm localized at 150 nm layer thickness (it is related to double perovskite material structure) and then 350 nm layer thickness (it showed a little generation rate in the 0D perovskite material structure). The maximum charge carrier generation ($6x10^{34}$ $m^{-3}s^{-1}$) occurred for the triple layer cell structure at the wavelength 350 nm in the double perovskite layer ($Cs_2InCoCl_6$). And the broadband photon absorbed in the visible region through the entire layers $CsGeCl_3$ (at 150 nm-thickness) and $Cs_2InCoCl_6$ (at 300 nm-thickness). While photon absorption and charge carrier generation became superior for the triple layer cell structure because of the inserted Cs_3BiBr_6 material. A pronounced maximum around 750-800 nm corresponds to the effective bandgap (~ 1.13 eV). Notably, significant generation is also observed closer to the rear interface, indicating that optimizing the back contact and minimizing recombination at this region will be crucial to ensure efficient charge collection for the triple layer cell structure (see Figure 8)

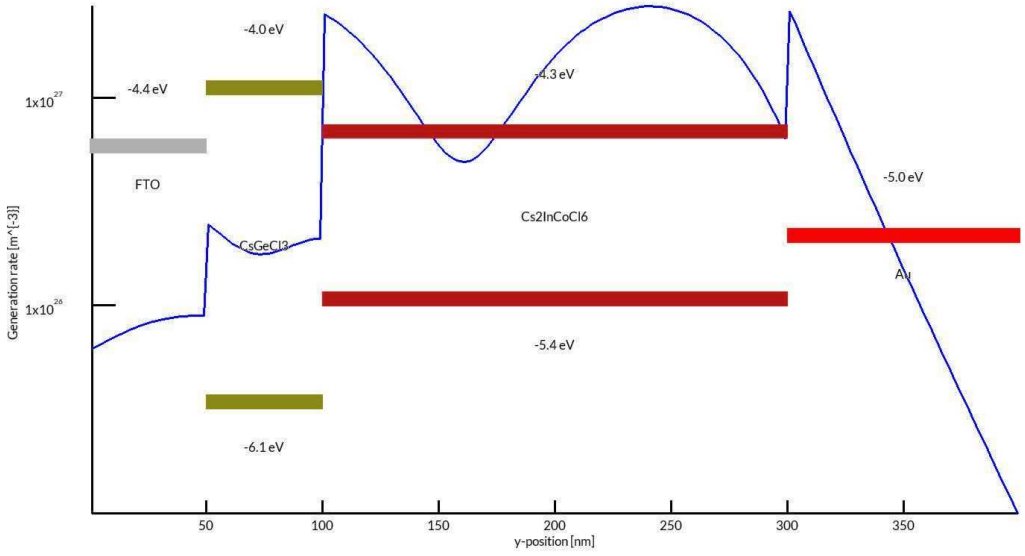


Figure 9. The charge carrier generation rate through the perovskite layers' thickness with respect to their energy levels for the structure without a zero-dimensional perovskite material layer.

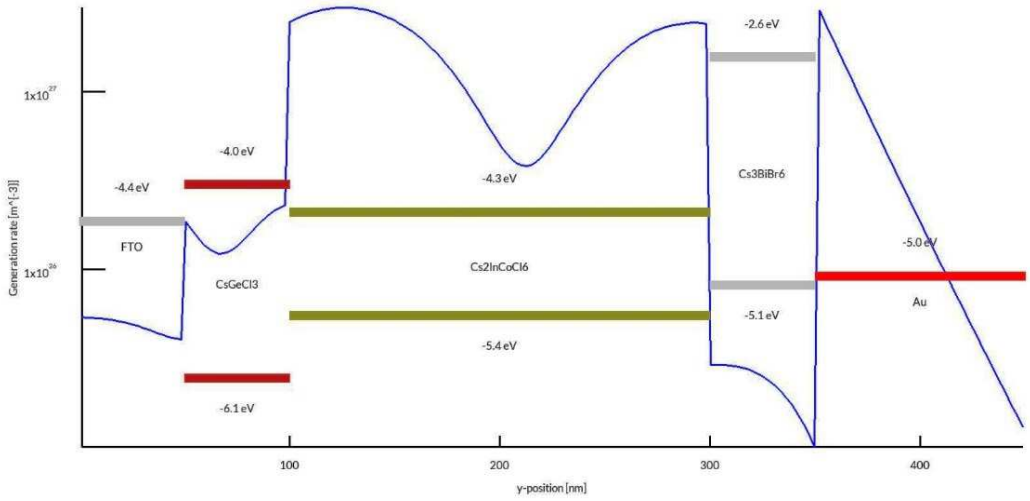


Figure 10. The charge carrier generation rate through the perovskite layers' thickness with respect to their energy levels for the structure without a zero-dimensional perovskite material layer

In PSCs, efficient carrier extraction is enabled by proper alignment of the perovskite conduction and valence band edges with the LUMO and HOMO levels of the transport materials, minimizing interfacial barriers and recombination losses. These processes are supported by the high carrier mobility and tunable bandgap of perovskites, which can be engineered through compositional and structural control (Iqbal et al. 2023)(Shi et al. 2018b). The absence of conventional ETL and HTL layers is an intentional design feature of this work. In the proposed $CsGeCl_3/Cs_2InCoCl_6/Cs_3BiBr_6$ heterostructure, $CsGeCl_3$ (electron affinity ~ 4 eV, wide band gap) effectively acts as an electron transport layer while also contributing to UV absorption, whereas Cs_3BiBr_6 (electron affinity ~ 2.6 eV, band gap ~ 2.5 eV) functions as a hole transport layer and electron-blocking layer. This integrated configuration enables efficient charge separation and transport through proper band alignment, eliminating the need for additional transport layers.

Figures 9 and 10 illustrate the charge carrier generation profile across the thickness of the PSC layers without and with 0D Cs_3BiBr_6 perovskite material, respectively. Alongside the generation rate distribution, the figure also aligns the energy levels of the different device layers, providing insight into the electronic structure and transport landscape. The generation rate, shown by the blue curve, varies strongly with depth, reaching its maximum value within the central region of the $Cs_2InCoCl_6$ layer, where absorption is more effective due to the direct band gap structure (see Figure 10). This indicates that the majority of photogenerated carriers originate within this region, consistent with its band alignment and optical activity. In contrast, the initial $CsGeCl_3$ layer near

the FTO substrate contributes comparatively little to overall generation, likely due to its less favorable absorption in the ultraviolet region and band offsets. The energy level alignment reveals that the conduction and valence band edges of $Cs_2InCoCl_6$ (at -4.3 eV and -5.4 eV, respectively) are well-positioned to facilitate charge transport towards the adjacent transport layers.

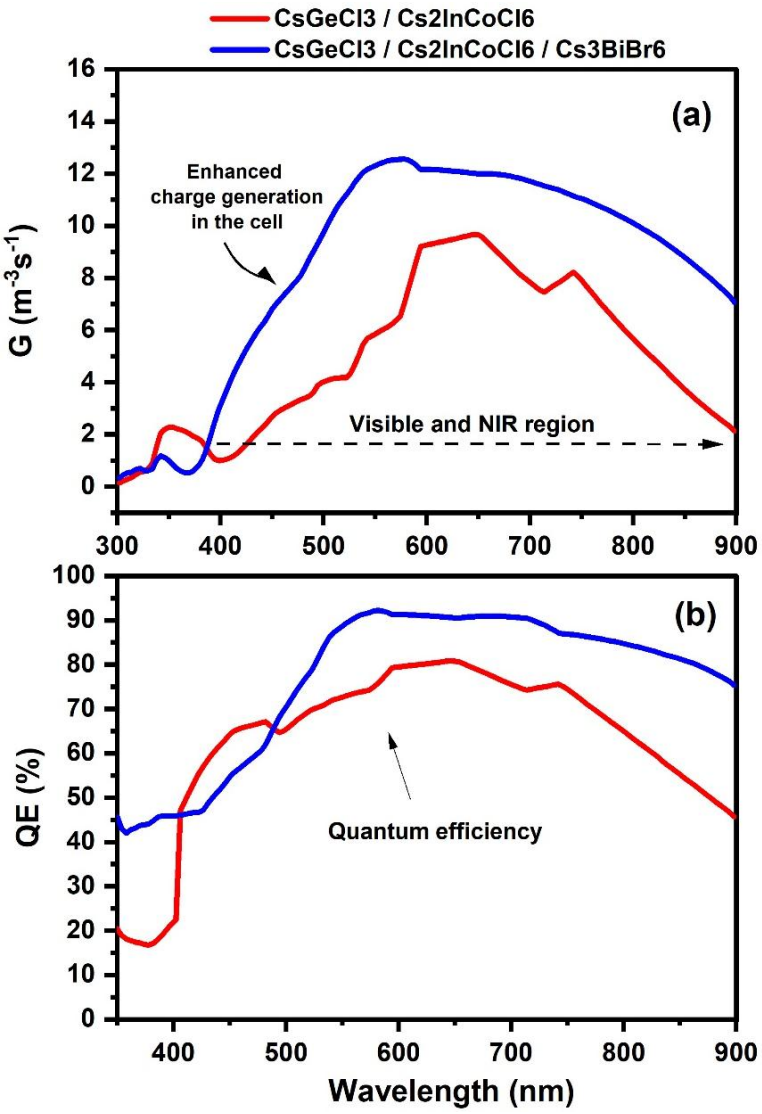


Figure 11. Effect of incorporating a zero-dimensional material layer on (a) the charge carrier generation rate and (b) the quantum efficiency of the cell when integrated as part of a triple-layer configuration in the perovskite solar cell structure. Results were obtained using OghmaNano simulation software over the wavelength range of 300–900 nm.

The generation rate spectrum and the quantum efficiency of the cells' structure with and without 0D Cs_3BiBr_6 perovskite layer are shown in Figure 11. The charge carrier generation rate (Figure 11a) demonstrates a significant enhancement across the visible and near-infrared (NIR) spectrum when Cs_3BiBr_6 is introduced as a third layer in the $CsGeCl_3/Cs_2InCoCl_6/Cs_3BiBr_6$ configuration.

The triple-layer device exhibits a higher and broader generation profile, particularly in the 400 - 800 nm range, indicating improved photon absorption and carrier photogeneration and it is matched with the above results. Correspondingly, the quantum efficiency (Figure 11b) shows a notable increase, with the triple-layer structure achieving peak values approaching 90%, while the double-layer counterpart remains consistently lower across the same wavelength range. The extended quantum efficiency into longer wavelengths up to 850 nm further confirms the enhanced light-harvesting capability of the device with Cs_3BiBr_6 and reduced surface defects in the layer. These improvements can be attributed to the superior light-scattering properties and reduced recombination at the interfaces provided by the zero-dimensional layer (Cs_3BiBr_6). Overall, the results suggest that integrating Cs_3BiBr_6 as part of a triple-layer architecture not only boosts charge generation but also significantly improves quantum efficiency, thereby offering a promising route toward higher-performance, lead-free PSCs.

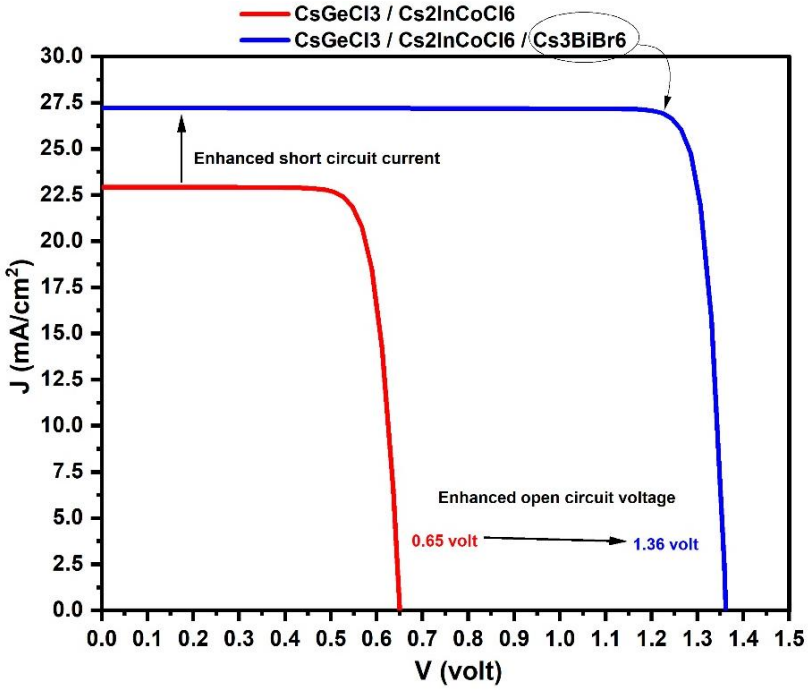


Figure 12. The current density-voltage of the perovskite solar cell for the two different structures, $CsGeCl_3/Cs_2InCoCl_6$ and $CsGeCl_3/Cs_2InCoCl_6/Cs_3BiBr_6$, with and without a zero-dimensional perovskite layer in the cell, respectively.

Figure 12 shows the simulated current-density voltage (J-V) results for both cell structures of $CsGeCl_3/Cs_2InCoCl_6$ and $CsGeCl_3/Cs_2InCoCl_6/Cs_3BiBr_6$. The results clearly indicate that the insertion of Cs3BiBr6 leads to simultaneous enhancements in both short-circuit current density

(J_{sc}) and open-circuit voltage (V_{oc}). Specifically, the V_{oc} increases significantly from ~ 0.65 V in the reference device to ~ 1.36 V with Cs3BiBr6, while Jsc improves from approximately 22.1 mA/cm^2 to 27.21 mA/cm^2. The J-V curve with Cs_3BiBr_6 also exhibits a more rectangular shape, implying reduced recombination losses, lower series resistance, and a higher fill factor. Collectively, these improvements translate into an estimated power conversion efficiency (PCE) increase of nearly threefold compared with the device without the 0D Cs_3BiBr_6 interlayer.

The apparent discrepancy between the band gap of $Cs_2InCoCl_6$ (1.13 eV) and the obtained Voc (1.36 eV) can be explained by the fact that the device is based on a $CsGeCl_3/Cs_2InCoCl_6/Cs_3BiBr_6$ (3D/Double/0D) heterostructure rather than a single absorber layer. The carrier generation is distributed across the structure, with strong absorption in the 300-400 nm range in $CsGeCl_3$ (~ 100 nm) and in the 400-900 nm range mainly within $Cs_2InCoCl_6$ (~ 150 nm), while Cs_3BiBr_6 contributes weakly at larger depths. The peak generation occurs in the central region of $Cs_2InCoCl_6$ due to its favorable absorption and direct band gap. However, the Voc is determined by the overall device energetics, including band alignment and quasi-Fermi level splitting across the heterostructure. Additionally, the wider band gap of $CsGeCl_3$ (2.12 eV) and its high absorption coefficient (~ $4x10^5$ cm^{-1}) in the high-energy region complement the absorption of $Cs_2InCoCl_6$ in the longer wavelength range. Therefore, the reported Voc reflects the combined optoelectronic behavior of the multilayer structure rather than being strictly limited by the band gap of $Cs_2InCoCl_6$ alone.

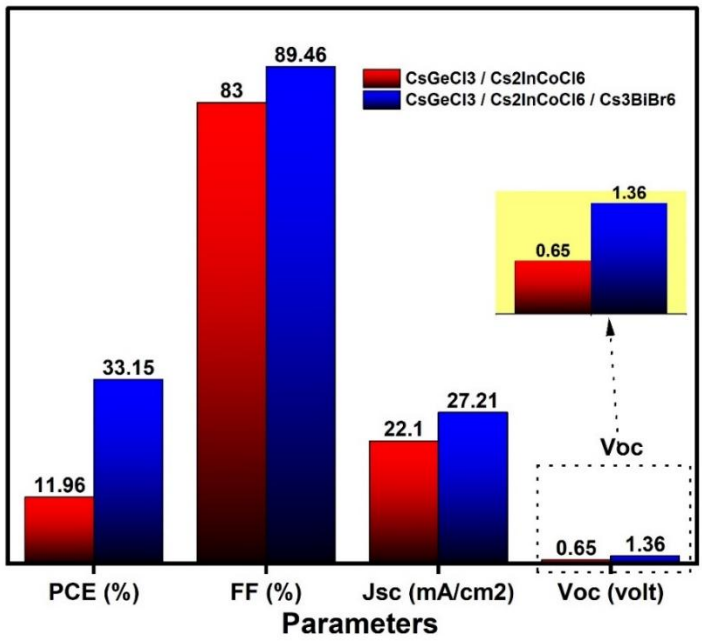


Figure 13. The cell performance parameters of the cell structures with and without 50 nm zero-dimensional perovskite layer (Cs_3BiBr_6)

The quantitative device parameters extracted from the J-V curves are summarized in Figure 13. Consistent with the trends observed in Figure 12, the insertion of the 50 nm Cs_3BiBr_6 interlayer yields substantial improvements in all photovoltaic parameters. The PCE increases nearly threefold, from 11.96% in the reference device to 33.15% with the interlayer. This dramatic enhancement is primarily driven by the large increase in V_{oc}, which rises from 0.65 V to 1.36 V, alongside a moderate gain in J_{sc} from 22.1 mA/cm^2 to 27.21 mA/cm^2. Additionally, the FF improves from 83% to 89.46% (see Table 2).

Table 2. Comparison of simulated performance parameters of perovskite solar cells with previously reported theoretical results.

Cell's Structure	**J_{sc} (mA/cm^2)**	**V_{oc} (volt)**	**FF (%)**	**PCE (%)**	**Research**	**Reference**
$CsGeCl_3/Cs_2InCoCl_6$	22.1	0.65	83	11.96	***Theoritical***	***Our work***
$CsGeCl_3/Cs_2InCoCl_6/Cs_3BiBr_6$	27.21	1.36	89.46	33.15	***Theoritical***	***Our work***
$C_{60}/CsSnBr_3/V_2O_5$	19.38	1.38	89.46	23.99	***Theoritical***	***(Shimul et al. 2025)***
$WS_2/CsGeCl_3/CBTS$	27.20	0.99	86	23.03	***Theoritical***	***(Mahedi et al. 2025)***
$TiO_2/Cs_2AgBiBr_6/Carbon$	12.11	1.69	88.79	18.21	***Theoritical***	***(Yang et al. 2025)***

4. Conclusions:

By incorporating the zero-dimensional perovskite structure, Cs_3BiBr_6 (0D), into the multi-layered structure of perovskite solar cells (PSCs), significant improvements are realized in terms of optical and electrical efficiency. From the numerical calculations using the software, OghmaNano, it was found that, although Cs_3BiBr_6 is largely transparent to incident photons and still exhibits slight absorption, it significantly alters the optical behavior of the system. The triple-layered structure suggested (50 nm-$CsGeCl_3$/200 nm-$Cs_2InCoCl_6$/50 nm- Cs_3BiBr_6) has lower reflectivity, high quantum efficiency of more than 90%, and excellent absorbance inside the $Cs_2InCoCl_6$ film. All these features have helped make significant improvements in the photovoltaic properties, which have been demonstrated through the increase of J_{sc} from 22.10 to 27.21 mA/cm^2, Voc from 0.65 to 1.36 V, fill factor from 83% to 89.46%, and PCE from 11.96% to 33.15%, i.e., an improvement of around 177%. Moreover, Cs_3BiBr_6 improves band alignment and reduces losses due to recombination, making it easier to extract charges effectively. Nonetheless, this study uses numerical simulations carried out under theoretical assumptions where all the material properties used are obtained from literature and theoretical results. The practical considerations, such as defects, interface loss, and stability, were not adequately addressed by experimental results, indicating that further experimental verification is required for this design.

Author Declaration:

I, Darko A. Noori, certify that I am the sole author of this work and have independently conducted the research, including the simulation design, data collection, data analysis, and interpretation of results. I also confirm that I have written and revised the manuscript in its entirety.

I take full responsibility for the content of this paper. I further certify that this work is original and has not been submitted to, nor published in, any other journal or publication, and will not be submitted elsewhere until a final decision has been made.

Conflict of interest:

The author has no conflicts to disclose.

Acknowledgment:

The author gratefully acknowledges all the support for this study from the Ministry of Higher Education and Scientific Research, Kurdish National Research Council (KNRC), Kurdistan Regional Government, and the University of Sulaimani.

References

Ai B, Fan Z, Wong ZJ (2022) Plasmonic–perovskite solar cells, light emitters, and sensors. Microsyst Nanoeng 8:5. https://doi.org/10.1038/s41378-021-00334-2

Alnujaim S, Bouhemadou A, Chegaar M, et al (2022) Density functional theory screening of some fundamental physical properties of Cs2InSbCl6 and Cs2InBiCl6 double perovskites. Eur Phys J B 95:114. https://doi.org/10.1140/epjb/s10051-022-00381-2

Azeem W, Shahzad MK, Hussain S, et al (2025) Investigation of semiconductor to metallic transitions of perovskite CsGeCl3 material through induced pressure: a DFT calculation for photovoltaic and optoelectronic applications. Mater Renew Sustain Energy 14:1. https://doi.org/10.1007/s40243-024-00276-5

Barichello J, Shankar G, Mariani P, et al (2024) Unveiling the potential of Cs2AgBiBr6 perovskites for next-generation see-through photovoltaics. Mater Today Energy 46:101725. https://doi.org/10.1016/j.mtener.2024.101725

Bothe K, Hinken D, Brendel R (2023) Extended *FF* and V_{OC} Parameterizations for Silicon Solar Cells. IEEE J Photovolt 13:787–792. https://doi.org/10.1109/JPHOTOV.2023.3309932

Chen Q, Wu J, Ou X, et al (2018) All-inorganic perovskite nanocrystal scintillators. Nature 561:88–93. https://doi.org/10.1038/s41586-018-0451-1

chrafih Y, Al-Hattab M, Rahmani K (2023) Thermodynamic, optical, and morphological studies of the Cs2AgBiX6 double perovskites (X = Cl, Br, and I): Insights from DFT study. J Alloys Compd 960:170650. https://doi.org/10.1016/j.jallcom.2023.170650

Faizan M, Bhamu KC, Murtaza G, et al (2021) Electronic and optical properties of vacancy ordered double perovskites A2BX6 (A = Rb, Cs; B = Sn, Pd, Pt; and X = Cl, Br, I): a first principles study. Sci Rep 11:6965. https://doi.org/10.1038/s41598-021-86145-x

Faizan M, Zhao G, Zhang T, et al (2024) Elastic and Thermoelectric Properties of Vacancy Ordered Double Perovskites A2BX6: A DFT Study. Acta Physico-Chimica Sinica 40:2303004. https://doi.org/10.3866/PKU.WHXB202303004

Gupta D, Mukhopadhyay S, Narayan KS (2010) Fill factor in organic solar cells. Solar Energy Materials and Solar Cells 94:1309–1313. https://doi.org/10.1016/J.SOLMAT.2008.06.001

Hao J, Hao H, Li J, et al (2018) Light Trapping Effect in Perovskite Solar Cells by the Addition of Ag Nanoparticles, Using Textured Substrates. Nanomaterials 8:815. https://doi.org/10.3390/nano8100815

Hwang I, McNeill CR, Greenham NC (2009) Drift-diffusion modeling of photocurrent transients in bulk heterojunction solar cells. J Appl Phys 106:. https://doi.org/10.1063/1.3247547

Iqbal Z, Zu F, Musiienko A, et al (2023) Interface Modification for Energy Level Alignment and Charge Extraction in $CsPbI_3$ Perovskite Solar Cells. ACS Energy Lett 8:4304–4314. https://doi.org/10.1021/acsenergylett.3c01522

Johnston MB, Herz LM (2016a) Hybrid Perovskites for Photovoltaics: Charge-Carrier Recombination, Diffusion, and Radiative Efficiencies. Acc Chem Res 49:146–154. https://doi.org/10.1021/acs.accounts.5b00411

Johnston MB, Herz LM (2016b) Hybrid Perovskites for Photovoltaics: Charge-Carrier Recombination, Diffusion, and Radiative Efficiencies. Acc Chem Res 49:146–154. https://doi.org/10.1021/acs.accounts.5b00411

Kaphle A, Echeverria E, Mcllroy DN, Hari P (2020) Enhancement in the performance of nanostructured CuO–ZnO solar cells by band alignment. RSC Adv 10:7839–7854. https://doi.org/10.1039/C9RA10771A

Kibbou M, Haman Z, Bouziani I, et al (2021) Cs2InGaX6 (X=Cl, Br, or I): Emergent Inorganic Halide Double Perovskites with enhanced optoelectronic characteristics. Current Applied Physics 21:50–57. https://doi.org/10.1016/j.cap.2020.10.007

Liang Y, Geng H, Yuan D, et al (2021) First-principles computations of elastic, electronic, and optical properties of zero-dimensional perovskite Cs3BiX6 (X = Br, Cl). Mater Chem Phys 262:124217. https://doi.org/10.1016/j.matchemphys.2020.124217

Luo J, Li S, Wu H, et al (2018) $Cs_2AgInCl_6$ Double Perovskite Single Crystals: Parity Forbidden Transitions and Their Application For Sensitive and Fast UV Photodetectors. ACS Photonics 5:398–405. https://doi.org/10.1021/acsphotonics.7b00837

Mäckel H, MacKenzie RCI (2018) Determination of Charge-Carrier Mobility in Disordered Thin-Film Solar Cells as a Function of Current Density. Phys Rev Appl 9:034020. https://doi.org/10.1103/PhysRevApplied.9.034020

Mahedi AH, Rahman MdS, Tarekuzzaman Md, et al (2025) Probing the impact of HTL layers on CsGeCl3-based perovskite solar cells for photovoltaic performance. Solar Energy 289:113338. https://doi.org/10.1016/j.solener.2025.113338

Marzouglal M, Souahlia A, Bessissa L, et al (2024) Prediction of power conversion efficiency parameter of inverted organic solar cells using artificial intelligence techniques. Sci Rep 14:25931. https://doi.org/10.1038/s41598-024-77112-3

Maurano A, Shuttle CG, Hamilton R, et al (2011) Transient Optoelectronic Analysis of Charge Carrier Losses in a Selenophene/Fullerene Blend Solar Cell. The Journal of Physical Chemistry C 115:5947–5957. https://doi.org/10.1021/jp109697w

Najarpour M, Matloub S (2025) Efficiency enhancement of dual-absorber EAGeI3/CsPbI3 perovskite solar cells via nanostructured interfaces and plasmonic nanoparticles. Sci Rep 15:34720. https://doi.org/10.1038/s41598-025-18330-1

Piprek J (ed) (2017) Handbook of Optoelectronic Device Modeling and Simulation. CRC Press, Boca Raton, FL : CRC Press, Taylor & Francis Group, [2017] |

Qu J, Wang Y, Li Z, et al (2025) Origin of Pressure-Induced Nonlinear Optical Property Enhancement in $CsGeCl_3$ Perovskite: $[GeCl_6]$ Octahedron Distortion and Band Gap Closing. J Am Chem Soc 147:6717–6726. https://doi.org/10.1021/jacs.4c16182

Richardson G, Walker A (2016) Drift Diffusion Modelling of Charge Transport in Photovoltaic Devices. In: Unconventional Thin Film Photovoltaics. The Royal Society of Chemistry, pp 297–331

Sahoo SK, Manoharan B, Sivakumar N (2018) Introduction: Why Perovskite and Perovskite Solar Cells? Perovskite Photovoltaics: Basic to Advanced Concepts and Implementation 1–24. https://doi.org/10.1016/B978-0-12-812915-9.00001-0

Seo D-K, Gupta N, Whangbo M-H, et al (1998) Pressure-Induced Changes in the Structure and Band Gap of $CsGeX_3$ (X = Cl, Br) Studied by Electronic Band Structure Calculations. Inorg Chem 37:407–410. https://doi.org/10.1021/ic970659e

Shahivandi H (2025) Comprehensive study of absorption coefficient and charge carrier generation in methylammonium lead iodide perovskite solar cells. Results Phys 76:108411. https://doi.org/10.1016/j.rinp.2025.108411

Sharma P, Ranjan P, Chakraborty T (2024) A density-functional-theory-based study of the lead-free perovskite materials $CsGeX_3$ and $CsGeX_2X'$ (X, X' = Cl, Br, I) for photovoltaic applications. J Phys D Appl Phys 57:505501. https://doi.org/10.1088/1361-6463/ad7a0a

Shi J, Li Y, Li Y, et al (2018a) From Ultrafast to Ultraslow: Charge-Carrier Dynamics of Perovskite Solar Cells. Joule 2:879–901. https://doi.org/10.1016/j.joule.2018.04.010

Shi J, Li Y, Li Y, et al (2018b) From Ultrafast to Ultraslow: Charge-Carrier Dynamics of Perovskite Solar Cells. Joule 2:879–901. https://doi.org/10.1016/j.joule.2018.04.010

Shimul AI, Islam ATMS, Ghosh A, et al (2025) Investigating charge transport layer flexibility for boosted performance in Lead-Free CsSnBr3-based perovskite solar cells. Comput Mater Sci 250:113701. https://doi.org/10.1016/j.commatsci.2025.113701

Shockley W, Read WT (1952) Statistics of the Recombinations of Holes and Electrons. Physical Review 87:835–842. https://doi.org/10.1103/PhysRev.87.835

Tang T-Y, Zhao X-H, Hu D-Y, et al (2022) An ab-initio investigation of novel double halide perovskite Cs2InCoX6(X=F, Cl, Br) materials with direct band structure and broadband light absorption. Mater Sci Semicond Process 152:107047. https://doi.org/10.1016/j.mssp.2022.107047

Thi Han N, Khuong Dien V, Lin M-F (2022a) Electronic and Optical Properties of $CsGeX_3$ (X= Cl, Br, and I) Compounds. ACS Omega 7:25210–25218. https://doi.org/10.1021/acsomega.2c02088

Thi Han N, Khuong Dien V, Lin M-F (2022b) Electronic and Optical Properties of $CsGeX_3$ (X= Cl, Br, and I) Compounds. ACS Omega 7:25210–25218. https://doi.org/10.1021/acsomega.2c02088

Tripathi MN, Saha A, Singh S (2019) Structural, elastic, electronic and optical properties of lead-free halide double perovskite Cs_2AgBiX_6 (X = Cl, Br, and I). Mater Res Express 6:115517. https://doi.org/10.1088/2053-1591/ab48ba

Wang D-L, Cui H-J, Hou G-J, et al (2016) Highly efficient light management for perovskite solar cells. Sci Rep 6:18922. https://doi.org/10.1038/srep18922

Yang H, Cai T, Dube L, Chen O (2022) Synthesis of double perovskite and quadruple perovskite nanocrystals through post-synthetic transformation reactions. Chem Sci 13:4874–4883. https://doi.org/10.1039/D2SC00574C

Yang W, Li W, Liu Q, Jin Y (2025) Design and simulation of gradient-structured Cs2AgBiBr6 carbon-based double perovskite solar cell for boosting photovoltaic performance. Solar Energy 290:113347. https://doi.org/10.1016/j.solener.2025.113347

Yang W, Yao Y, Wu C-Q (2015) Origin of the high open circuit voltage in planar heterojunction perovskite solar cells: Role of the reduced bimolecular recombination. J Appl Phys 117:. https://doi.org/10.1063/1.4913519

Zhao Y, Xiang H, Ran R, et al (2023) Beyond two-dimension: One- and zero-dimensional halide perovskites as new-generation passivators for high-performance perovskite solar cells. Journal of Energy Chemistry 83:189–208. https://doi.org/10.1016/j.jechem.2023.04.025

Zhou X, Jankowska J, Dong H, Prezhdo O V. (2018) Recent theoretical progress in the development of perovskite photovoltaic materials. Journal of Energy Chemistry 27:637–649. https://doi.org/10.1016/j.jechem.2017.10.010

Zhu B, Chen L, Ye S, Luo W (2023) The Light-Trapping Character of Pit Arrays on the Surface of Solar Cells. Photonics 10:855. https://doi.org/10.3390/photonics10070855

Supplementary Files

This is a list of supplementary files associated with this preprint. Click to download.

- nabsorbanceofthesamples.opju
- Graphs.opju
- Responsewithhighlgihtedtextinmanuscript.rar